Journal of Applied Polymer Science

REVIEW

Polymer nanogenerators: Opportunities and challenges for large-scale applications

Aurelia Chi Wang,[1] Changsheng Wu,[1] Dario Pisignano,[2,3] Zhong Lin Wang,[1] Luana Persano [2]

[1]School of Materials Science and Engineering, Nanoscience Department, Georgia Institute of Technology, Atlanta, Georgia 30332-0245

[2]NEST, Istituto Nanoscienze-CNR, Piazza S. Silvestro 12, Pisa I-56127, Italy

[3]Dipartimento di Matematica e Fisica "Ennio De Giorgi," Università del Salento, via Arnesano I-73100, Lecce, Italy

Correspondence to: Z. L. Wang (E-mail: zhong.wang@mse.gatech.edu) and L. Persano (E-mail: luana.persano@nano.cnr.it)

ABSTRACT: Technologies for energy harvesting from objects in motion are gaining a continuously increasing interest to directly power wearable electronics, sensors, and wireless transmitters. New networks where things will be uniquely identified and interconnected will require key enabling technologies, particularly cheap, flexible generators of renewable energy, conformable to any solid surface, to power independently individual objects and data transmission. Polymer-based nanogenerators (PNGs), capable of converting mechanical energy into electricity, have exact features to fulfill these requirements. This article highlights advances in PNGs with focus on material chemistries and geometrical features, device design strategies, and performances. Representative examples of applications which show large-scale capability are reported. Concluding sections summarize the key challenges and the commercialization perspectives of PNGs for use in real life applications. © 2017 Wiley Periodicals, Inc. J. Appl. Polym. Sci. **2017**, *134*, 45674.

KEYWORDS: applications; electrospinning; films; synthesis and processing techniques

Received 15 June 2017; accepted 26 July 2017

DOI: 10.1002/app.45674

INTRODUCTION

Energy harvesting is the process enabling the transformation of various forms of renewable energy, for example, solar, thermal, electrostatic, and kinetic energy, in electrical energy (Figure 1). The forthcoming "Internet of Things" creating a network where bodies and objects are uniquely identified and interconnected through data flows, will allow to monitor continuously several activities and applications determining (i) new rules for security, health, and environment check and (ii) new requirements for powering units. The integration of systems allowing for harvesting energy from the environment or from surrounding objects in motion can represent a sustainable option for directly powering wearable electronics, wireless sensors, structure- and health-monitoring devices in the "Internet of Things" networks. Nanogenerators (NGs), converting mechanical energy into electricity are relatively simple in device design, capable of high-efficiency energy harvesting, and do not require high frequency mechanical input to be viable. The first NG was demonstrated by Wang and Song in 2006.[1] The device exploited the piezoelectric effect generated by the deflection, at nanoscale, of an aligned arrays of zinc oxide nanowires definitely evidencing the potentiality of converting forms of mechanical energy into electricity for powering nanodevices. This pioneering work was followed by an intense research activity leading to the realization of several NGs with different materials, device design, and functionalities. In particular, nanomaterials demonstrated the potential to optimize the output performances and to expand the range of device structures, while advances in available fabrication techniques enabled the incorporation of inorganic nanomaterials onto compliant substrates,[2] thus creating opportunities for flexible and stretchable devices unattainable with traditional approaches. Polymers are especially promising for NGs, because they combine structural flexibility and ease of processing with large sensitive areas, simplicity in device design, and associated potential for low-cost implementation. They can be easily tailored at the nanoscale by room temperature processes, and technologies for scaling up the fabrication process of the related nanomaterials are already viable on the market[3] thus making polymer-based NGs (PNGs) good candidates for real-life applications. In addition, they are lead-free and they can conform to the surface of various objects including human organs and skin, suggesting bio/eco-compatible options for their use.[4] PNGs can generate electrical power from movements of the human body, vibrations, contact among dissimilar materials and environmental sources such as sun, wind, water flows, and others. Among them, mechanical sources are the most ubiquitous and accessible ones, and the associated devices can be easily integrated with wearable electronic systems also for remote monitoring and sensing. The transducing mechanisms so far explored are

Aurelia Chi Wang received her BS in Biochemistry in 2013 from the Georgia Institute of Technology. After working at Medical Neurogenetics from 2014 to 2016, she returned to the Georgia Institute of Technology to work on her doctoral research under the supervision of Prof. Zhiqun Lin and Prof. Zhong Lin Wang. Her research interests include nanomaterials, polymer-based energy harvesting, and self-powered smart device design.

Changsheng Wu received his Bachelor of Engineering in Engineering Science Programme from National University of Singapore in 2013. He is currently pursuing a Ph.D. in Materials Science and Engineering at Georgia Institute of Technology under the supervision of Prof. Zhong Lin Wang. His research interests include energy harvesting, self-powered electronics, and additive manufacturing.

Dario Pisignano, PhD in Physics, is Associate Professor at the University of Salento. He coordinates an interdisciplinary group working on Nanotechnologies on Soft Matter at the University of Salento and at CNR-Nanoscience Institute. His research activity is focused on the development of advanced polymer processing and lithographic approaches, electrospinning, and soft lithographies, for realizing micronanostructured devices, organic lasers, and functional systems. He has been awarded the "Young researcher" Prize at the National INFM Meeting, the International Obducat Prize for Nanoimprinting Lithography, the National Award "Future in Research" of the Ministry of Education, University and Research, and the "Sergio Panizza" Award for Optoelectronics and Photonics (Italian Physics Society, SIF). He is the recipient of the NANO-JETS ERC Ideas Starting Grant, whose details can be found at: http://www.nanojets.eu.

Zhong Lin Wang received his PhD from Arizona State University in physics. He now is the Hightower Chair in Materials Science and Engineering, Regents' Professor, Engineering Distinguished Professor and Director, Center for Nanostructure Characterization, at Georgia Tech. Dr. Wang has made original and innovative contributions to the synthesis, discovery, characterization, and understanding of fundamental physical properties of oxide nanobelts and nanowires, as well as applications of nanowires in energy sciences, electronics, optoelectronics, and biological science. His discovery and breakthroughs in developing nanogenerators established the principle and technological road map for harvesting mechanical energy from environment and biological systems for powering personal electronics. His research on self-powered nanosystems has inspired the worldwide effort in academia and industry for studying energy for micronanosystems, which is now a distinct disciplinary in energy research and future sensor networks. He coined and pioneered the field of piezotronics and piezo-phototronics by introducing piezoelectric potential gated charge transport process in fabricating new electronic and optoelectronic devices. Details can be found at: http://www.nanoscience.gatech.edu.

Luana Persano, PhD in Innovative Materials and Technologies, is staff researcher at CNR-Nanoscience Institute. She has been Marie-Curie fellow at FORTH, Greece, and visiting scientist at Harvard University and University of Illinois. Her research interests include nanomanufacturing and lithographic processes onto nanocomposites and active materials in the form of films, NPs and fibers, and the implementation of nanophotonic and piezoelectric devices based on them. She is co-founder of Soft Materials and Technologies, a company focused on the development of micro and nanotechnologies for the production of nanostructured soft materials through the exploitation of unconventional soft lithography and electric-voltage driven techniques.

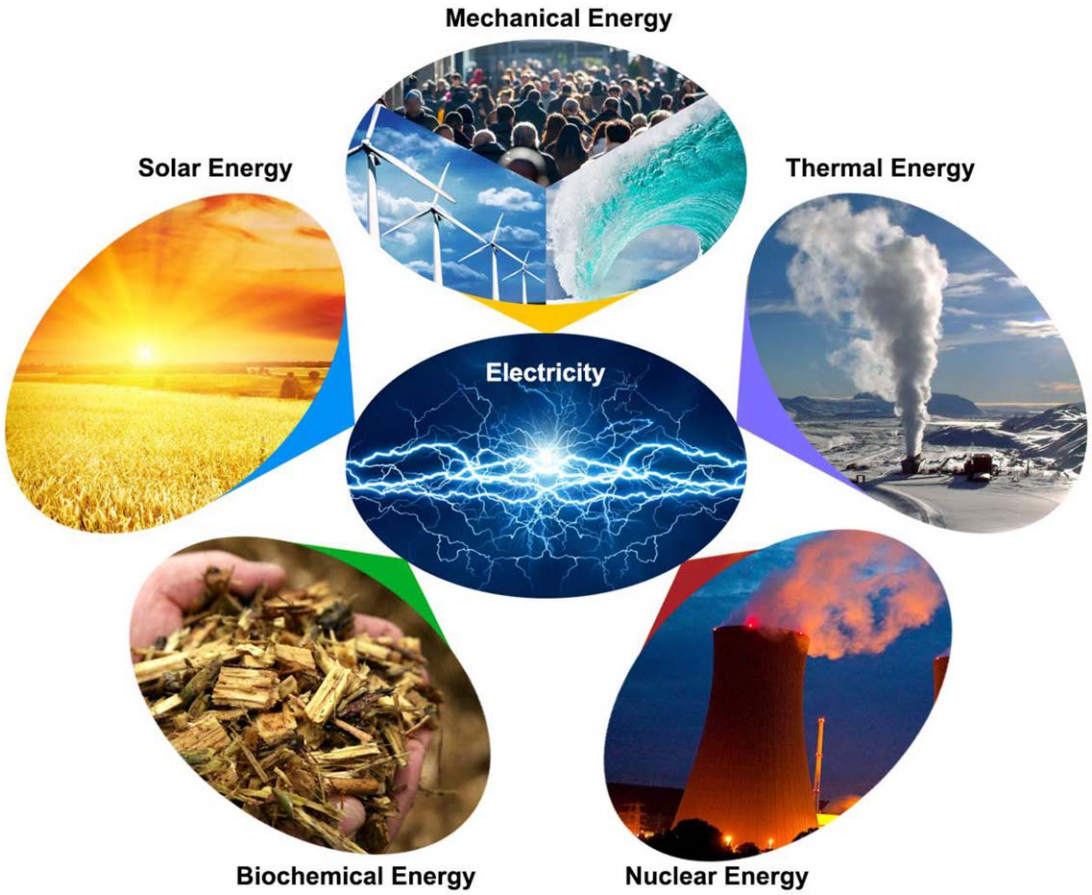

Figure 1. Major energy harvesting technologies for electricity generation. [Color figure can be viewed at wileyonlinelibrary.com]

(i) piezoelectricity, (ii) triboelectricy, (iii) electrostatic, and (iv) electromagnetic induction. This review highlights advances in mechanical PNGs over the past 5 years with focus on material chemistries (organics and composites) and geometrical features (nanostructures and thin films), device design strategies, and performances. Representative examples of applications which show large-scale capability are reported and the key challenges for device commercialization are highlighted. The collective results suggest a promising future for the integration of PNGs harvesting energy from mechanical motion in complex networks for data exchange.

POLYMER-BASED NGS

Piezoelectric NGs

The word piezoelectricity, derived from the Greek "piezein" which means "to press" and "ēlektron" which means "amber", means stress-induced electricity. The piezoelectric effect represents the capability of certain materials to generate spatially separated electrical charges of opposite sign, in response to an external force producing a mechanical deformation. The accumulation of electrical charges at two ends of the material body allows the formation of an electric dipole resulting in the formation of a piezopotential. This effect can be observed in materials whose crystalline state has no center of symmetry (so-called noncentrosymmetric), including polymers and biological systems.[5] By connecting the material to an external load, and in absence of short-circuited contacts, free electrons flow through the external circuit in order to balance the polarization charges and achieve a new equilibrium state. The application of a dynamic strain cause indeed the formation of a pulsed steady stream of current flowing through the external circuits that can be recorded and stored. Polymer-based NGs generally consists of a polymer layer with electrical contacts at the ends and positioned onto flexible/stretchable substrates. In the last years, several materials and device design have been explored in order to (i) harvest various forms of energy from the environment such as vibrations, sound, water flow, and mechanical pressure; (ii) improve the output performances, device stability, and lifetime; and (iii) match the device mechanics with structural requirements related to specific working conditions. Polyvinylidenefluoride (PVDF) and its copolymers are by far the most used piezoelectric polymers because of their advantageous properties in terms of structural flexibility, ease of processing, good chemical resistance to solvents, acids, and bases, and mechanical strength. Their high fracture strain (about 2%) makes them very promising candidates for the realization of flexible, bendable, and stretchable energy harvesting devices, especially when compared with inorganic ceramics and metal-oxides such as zinc oxide (ZnO), lead zirconate titanate, and barium titatane ($BaTiO_3$) which are characterized by an intrinsic fracture strain <1%.[6] The plastic behavior allows high-throughput processing[7] based on moulding, casting, drawing, and spinning

technologies. In addition, being biocompatible, they can be safely used in biological systems to make sensors and self-charging implantable devices. However, achieving good performance requires electrical poling to align dipoles of the polar β-phase in the direction orthogonal to the film plane,[8] thus limiting engineering design options and, at the same time, requiring multiple preparatory steps and additional cost. Emerging techniques of nano- and microfabrication show the potential to improve the piezoelectric response and expand the range of material geometries and device structures that can be considered. For example, electrospinning technologies which are based on the uniaxial elongation of a polymer jet in the presence of an intense electric field (typically 10^5–10^7 V/m) applied between the spinneret and a conductive collector, can produce piezoelectric materials in the form of nanofibers and nanowires with enhanced piezoelectric properties. The combination of strong stretching forces and high electric fields naturally cause local poling and, by consequence, superior performances. Nanofibers of PVDF and its copolymers with different shapes and organization have been reported. Individual suspended fibers of poly(vinylidenefluoride-*co*-trifluoroethylene) (PVDF-TrFE) with diameter 400–600 nm and length in the millimeter scale, generate open-circuit voltage of 60 μV under well-defined levels of displacement in the submicroscale. Density functional theory has been used to calculate the piezoelectric coefficients and the full piezoelectric tensor for different copolymer configurations, also highlighting the role of shear forces contributions in flexible polymeric nanobeams.[9] By using properly designed collectors, fibers can be arranged in various forms such as random mats,[10] aligned strands,[11,12] highly aligned arrays,[13] ribbonds and yarns[14] realized by twisting ribbons. Interesting, Baniasadi *et al.* have found that the twisting process of aligned ribbons of PVDF-TrFE increases up to a factor of 2 the strain to failure, strength, and toughness of the materials. In addition, coils fabricated by twisting the yarns [Figure 2(a)] exhibit an additional enhancement of the strain to failure (by a factor 4 with respect to yarn) with a maximum strain up to ~740%.[14] Ribbons generate an output voltage of tens of mV under bending while the combination of the piezoelectric charges and friction under stretching are considered to contribute to the enhancement of the mechanical properties though the increase of shear and compressive forces between nanofibers. Other advantages of the electrospinning technology in the field of piezoelectricity are the high yield and throughput, the high aspect ratio (larger than 10^5),[11] the capability to make composite materials, and the low cost associated with the process. On the other hand, applications are still limited due to the lack of reliable and affordable approaches which, combined with theoretical modeling and *in situ* monitoring, allow good control on the material uniformity and properties.[3] Another technology capable of producing piezoelectric PVDF in the form of very long filaments with different cross-sectional shape and without the need of extra electrical poling is thermal drawing. Figure 2(b) reports a scheme of the fabrication procedure of nanoribbons of PVDF embedded in poly(ether sulfone) to realize the preform to be successively used in fiber drawing.[15] Several fiber drawing steps with temperature up to 285 °C and feeding speed of 8 mm/s are required to achieve PVDF ribbons with final diameter ~300 nm.[15] The poly(ether sulfone) cladding is finally removed by immersion in a nonsolvent for PVDF. The concomitant effect of stress and high temperature exerted during the process favors the formation of the PVDF γ-phase that, although has lower polarity when compared to the β-phase typically achieved during the electrospinning process, has high Curie temperature thus enabling stable operation also in harsh environmental conditions. An alternative approach capable to fabricate polar PVDF-based materials without additional poling is represented by the electrohydrodynamic pulling technology.[16] As schematically shown in Figure 2(c), a direct current (dc) electric field (600 V) is applied to the two opposite surfaces of a prepatterned film of PVDF-TrFE maintained at temperature slight above the glass transition temperature of the polymer (150 °C) and sandwiched between two conductive layers. Kapton spacers are used to ensure the proper air clearance between the two electrodes. During the process, the formed Maxwell force pulls the polymer micropillars upward. Their diameters reduce by a factor 2 (~8 μm) and their length almost double, while the molecular dipoles align vertically. Once the system is cooled, the material is frozen in the final configuration. The main advantages of this technology are that (i) no further processing is needed to fabricate the device since the same electrodes used to form the pillars will then constitute the electrodes of the final device and (ii) the high adhesion between the P(VDF-TrFE) microfiber array and the top and bottom contact provides improved performances. A NG with effective area of 10 mm × 10 mm excited with a periodic compressive load of 30 N at 60 Hz generates a voltage of 5.0 V with current of few μA.[16] The energy produced, after rectification and storage, was used to drive a seven segment display. A strategy that can be adopted to further improve the piezoelectric performances is to increase the material surface area such as in sponge-like architectures. Mesoporous film of PVDF realized by casting a mixture of PVDF/ZnO nanoparticles (NPs) and subsequent wet etching to selectively remove the NPs [scheme in Figure 2(d); (i)] generate up to 11 V under acoustic wave impact at 60 Hz, *albeit* a poling procedure was applied at 60 V μm^{-1} for 2 h before testing the NG performances.[17] Melt wetting and molding procedures with anodized alumina templates have been also largely used to produce array of isolated nanowire[19] and nanotubes[20] with reasonable poling field (35 V μm^{-1}). However, nanopatterning and size confinement approaches for the realization of polymer piezoelectric nanostructures have limitations in terms of aspect ratio, yield, geometry control, and flexibility in the device design.[15] Composite materials made by mixing PVDF with inorganic systems[21] and two-dimensional materials[22,23] have been demonstrated as valuable strategy to improve the piezoelectric properties. Perovskite $BaTiO_3$ NPs, which are lead-free and exhibit excellent piezoelectric features (d_{33} = 30–100 pm/V)[24] are typically mixed in the polymer solution with a relative concentration of 20%–50% wt and then deposited by spin-coating. Curing processes at 80 °C under ambient conditions may follow to induce the formation of hemispherical $BaTiO_3$ clusters which decorate the film surface and are found to strongly improve the piezoelectric power generation by boosting the total dipole

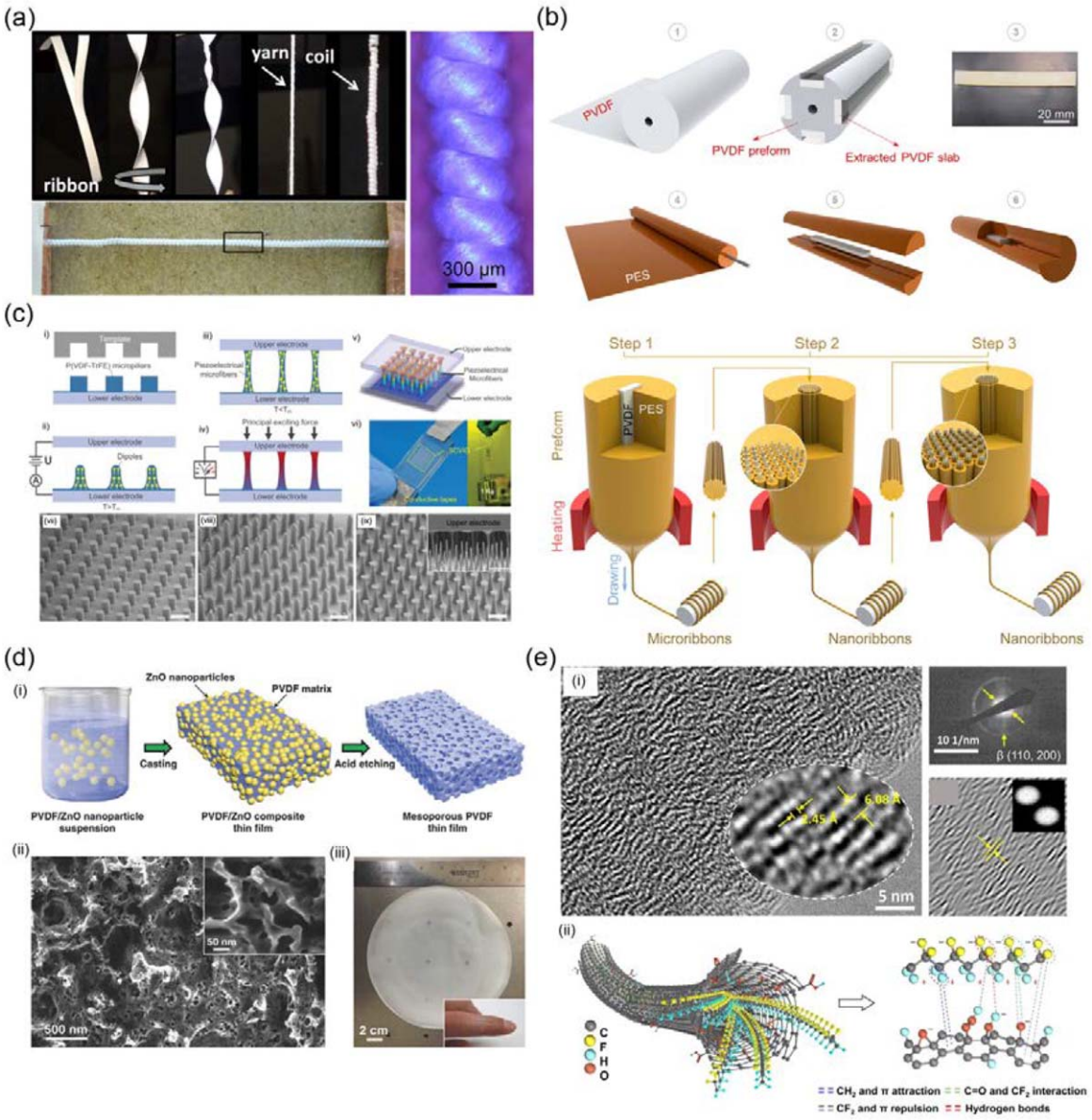

Figure 2. Piezoelectric materials. (a) Twisting process used to fabricate yarns and coils from electrospun ribbons. Reprinted with permission from Ref. 14, Copyright (2015) American Chemical Society. (b) Scheme of the nanofabrication technique used for producing kilometer-long piezoelectric nanoribbons by thermal drawing (1–6). The fabrication steps used to embed PVDF ribbon in poly(ether sulfone) (PES) preform, which is a macroscopic copy of the final nanoribbons. Step 1–3: Iterative fiber drawing process to achieve ribbons at the nanoscale. Reprinted with permission from Ref. 15, Copyright (2014) American Chemical Society. (c) Scheme of the electrohydrodynamic pulling process used to realize piezoelectric micropillars (i–iv) and the piezoelectric device (v and vi). SEM micrographs of the polymer during the pillar formation. Scale bars: 30 micrometers. (vii–xi). Reproduced with permission from Ref. 16, Copyright (2015) The Royal Society of Chemistry. (d) Processing (i) and morphology (ii) of mesoporous PVDF thin films (iii). Reprinted with permission from Ref. 17, Copyright (2014) John Wiley & Sons. (e) High-resolution TEM image of the PVDF/GO nanofiber (i) and the related three-dimensional molecular model (ii). Adapted with permission from Ref. 18, Copyright (2017) American Chemical Society. [Color figure can be viewed at wileyonlinelibrary.com]

moment inside the cluster.[21] Open-circuit voltage of ~75 V and short-circuit current of ~15 μA are generated under a compressive pressure of ~0.23 MPa, while 5 V are generated during dynamic bending. Improved output dynamic response can be accomplished in similar systems upon increasing by a factor of 10 the electric field during the post-process poling (100 MV/m), which results in an output voltage of about 10 V during bending.[25] The incorporation of inorganic NPs at high weight percentage in polymer matrix then leads to strongly improved NG performance, while preserving the flexibility and the light weight of such devices. However, it is well known that the rheological behavior of the resulting composites might be dramatically affected by the inclusion of the NPs. In particular, the increase of the overall viscosity, the delayed thermomechanical

response,[26] and the control on the dispersion uniformity may strongly limit the possibility of shaping composites in the form of nanostructures or wires, which would benefit of an enhanced surface active area and additional possibilities of device design. In this respect, the implementation of low-temperature methods for the *in situ* synthesis of $BaTiO_3$ NPs[27,28] into a preformed polymer matrix, analogously to previous studies on light emissive nanocrystals,[29,30] is especially interesting in view of realizing energy harvesting composites. Also, graphene and its derivatives have recently emerged as alternative fillers for PVDF.[23] The resulting materials, with a typical graphene content <5% wt, show improved thermal stability in air and nitrogen environment, an increase of the elastic and flexural modulus and a reduction of the elongation at break.[31] In addition, an enhancement of the polar β-phase content has been determined and correlated to the presence of the graphene fillers, which induce a reorientation of the β-phase nanocrystals during their formation.[18,32] Liu *et al.*[18] reported on electrospun core−shell fibers of PVDF chemically wrapped by graphene oxide (GO) lamellae, in which the polar β-phase nanocrystals are formed and uniaxially oriented by the synergistic effect of mechanical stretching, high-voltage alignment, and chemical interactions. So far, this material exhibits the larger measured out-of-plane piezoelectric constant, $d_{33} = -93.75$ pm/V (at 1% wt GO). The dramatic enhancement in piezoelectricity is elucidated by a three-dimensional molecular modeling [Figure 2(e); (ii)] indicating that during the electrospinning process, the GO lamellae move to the surface of the nanofibers because of internal radial orientation of the electrostatic field and of rapid evaporation of the solvents. Electrostatic attraction/repulsion between the delocalized π-electrons in GO and the —CH_2/—CF_2 dipoles of PVDF anchors the PVDF chains to the GO lamellae. Hydrogen bonds are formed between the CF_2 groups of PVDF and the —COOH/—OH bonds in the GO lamellae, contributing to the uniaxial alignment of the PVDF chains during the electrospinning process. A similar system was used by Park *et al.* to introduce a human skin-inspired multimodal e-skins. The device is based on flexible and microstructured composite films of PVDF/rGO (rGO, reduced GO) with an active area of 1 cm^2 which can detect and discriminate between multiple spatiotemporal tactile stimuli including the piezoelectric detection of dynamic touch and acoustic waves.[22] Alternative materials to the PVDF family are mainly based on composite multimaterial elements, including hybrid organic–inorganic systems such as $BaTiO_3$/polyethylene glycol diacrylate,[33] $BaTiO_3$/poly(dimethylsiloxane) (PDMS) foams,[34] cellular polypropylene piezoelectrets,[35] and arrays of nylon-11.[36]

A very important role in the device design for piezoelectric NGs is played by the substrate positioned below the active material. In particular, when bending the device, the thickness and the Young's modulus of the substrate strongly influences the position of the neutral strain axis and correspondingly the strain values in the active layer. Generally, in full polymer systems, thicker plastic substrates corresponds to larger electrical output.[13] Lee *et al.* investigated the effect of the substrate material and thickness on the response of a PVDF based NG under sound-driven mechanical vibrations.[37] They found that the device performances depend on the thickness of the flexible substrate underneath and are related to the different amount of the stress transferred by the substrate to the piezoelectric material. When designing stretchable NGs instead, both a proper selection of all the material constituting the device (including electrodes and interconnections) and of the structural design must be performed in order to ensure device operation, long-term stability, and output performances.[6] Duan *et al.*[12] reported on a controllable buckled array of PVDF nanofibers made by electrohydrodynamic direct-writing onto prestrained PDMS substrates. Authors found that upon release of the PDMS substrate, fibers form "in or out-of-surface" buckling shapes depending on the electrospinning parameters used. An energy harvester composed of 120 direct-written in-surface buckled PVDF fibers with a length of 3 cm, periodically stretched and released (30% strain at frequency of 0.5 Hz), can generate current and voltage of ≈1.2 nA and ≈40 mV, respectively. An hyperstretchable device (≈200% strain) with output voltage of ≈4 V and current of ≈500 nA was reported by Jeon *et al.*[38] Hyperstrechability was achieved by processing high stretchable materials in the form of a monolithic assembly. Very long and stretchable nanowire percolation electrodes were directly transferred on both sides of a rubber-based piezoelectric elastic material composed of lead magnesium niobate-lead titanate (PMN-PT) particles and multiwalled carbon nanotubes in a silicone elastomer matrix. The combination of (i) high performing material (PMN-PT particles with $d_{33} = 690$ pC N^{-1} and electromechanical coupling factor, $k_{33} = 0.73$) and (ii) very large strain enables high output performances and device stability also under twisting, folding, and crumping deformation.[38]

In piezoelectric PNGs, electrodes can be shaped in various forms and several metal, polymeric, and hybrid materials have been so far used. The electrode design depends mainly on the piezoelectric material properties and on the mechanism used to transduce electricity. Unlike crystalline inorganic solids, for which piezoelectricity is generally achieved by strain along the direction of the spontaneous polarization vector and is theoretically described by an uniaxial model, in polymeric systems, which are intrinsically flexible, the stress applied along one axis also causes remarkable deformations along perpendicular directions.[9] More complex transverse contributions can be then taken into account while designing the device, and the electrodes can be positioned to collect piezo-voltage along a direction either perpendicular[9] [Figure 3(a)] or parallel to the applied stress.[42] Gold, liquid Ag paste, and Al foils are the most used metals although the requirements for transparent and fully flexible, stretchable NGs have increased the use of alternative materials such as PEDOT,[43] graphene,[44] and Ag nanowires.[38] Electrodes can be also nanostructured in order to increase the surface area in contact with the active layer. Li *et al.* reported an interesting example of wearable piezoelectric device assembled by a one-step continuous electrospinning method and where the PVDF nanofiber membrane is sandwiched between two PVDF-rGO nanofibers electrode [Figure 3(b); (i)].[39] The device exhibits high flexibility, lightness, stretchability, and operational stability. The output voltage is as large as 46 V and the power density is 18.1 μW cm^{-2}. Nanoribbon and fiber-based piezoelectric elements can be also encapsulated into polymers or

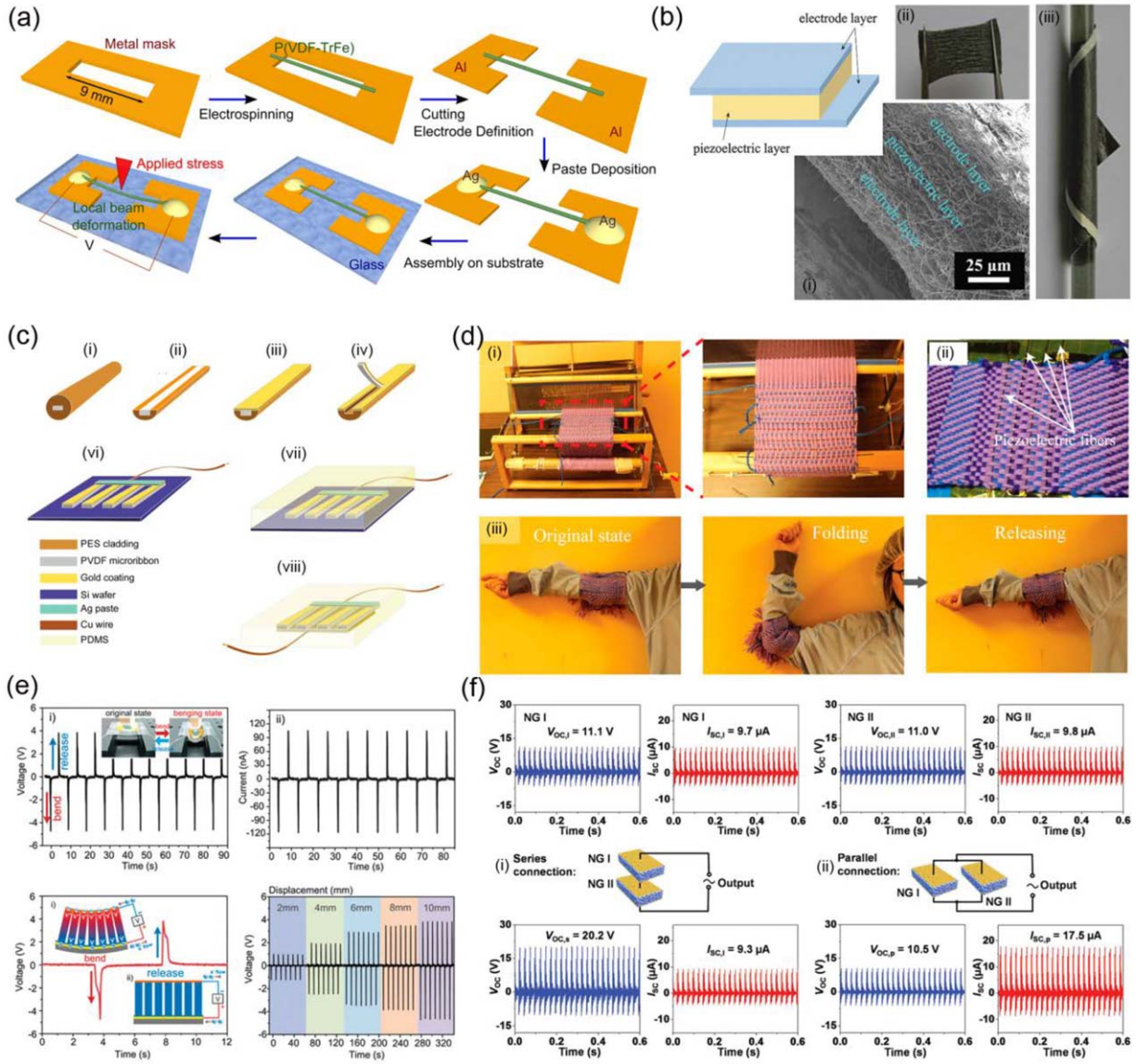

Figure 3. Piezoelectric nanogenerator. (a) Process schematics illustrating the fabrication steps for nanogenerators based on suspended PVDF-TrFE nanobeams. Reprinted with permission from Ref. 9, Copyright (2016) Weinheim: Wiley-VCH. (b) Schematic of a device with top and bottom contact. SEM cross section (i) and photographs (ii and iii) of the same device assembled by using a continuous electrospinning method. Reproduced with permission from Ref. 39, Copyright (2016) The Royal Society of Chemistry. (c) Fabrication process for a device produced using microribbons. Reprinted with permission from Ref. 15, Copyright (2014) American Chemical Society. (d) Photograph of the dobby loom (i) used to weave piezoelectric fibers into a cotton textile (ii) and its use in 90° folding-release action of the elbow (iii). Reprinted with permission from Ref. 40, Copyright (2017) American Chemical Society. (e) Output response of a flexural sensor based on vertically aligned nanowires of PVDF-TrFE upon bending/release motion. Reproduced with permission of from Ref. 41 Copyright (2015) The Royal Society of Chemistry. (f) Voltage and current outputs of individual nanogenerators (NGI and NGII). Voltage and current of the same while connected in series (i) and in parallel (ii). Reprinted with permission from Ref. 17, Copyright (2014) John Wiley & Sons. [Color figure can be viewed at wileyonlinelibrary.com]

fabrics for successive device integration. Figure 3(c,d) shows examples of the fabrication process used by Lu *et al.* to make NGs based on nanoribbons of PVDF with gold and Ag paste electrodes fully encapsulated within two PDMS layers and of piezoelectric fibers of PVDF/CNT made first by fiber drawing and then woven into a cotton textile by using a dobby loom system, respectively.[40]

The device performances of polymer-based piezoelectric NGs have been tested under dynamic solicitation through bending with typical frequencies of 1–5 Hz [Figure 3(e)],[41] stretching,[13,45] compressive forces,[46] vibration,[13] and surface oscillation.[17] Multiple NGs can be connected in series and in parallel [Figure 3(f)] and integrated into one system to operate synchronically.

Triboelectric NGs

Triboelectric NGs (TENGs), first invented in 2012, operate based on the triboelectric effect in which electrical charges are

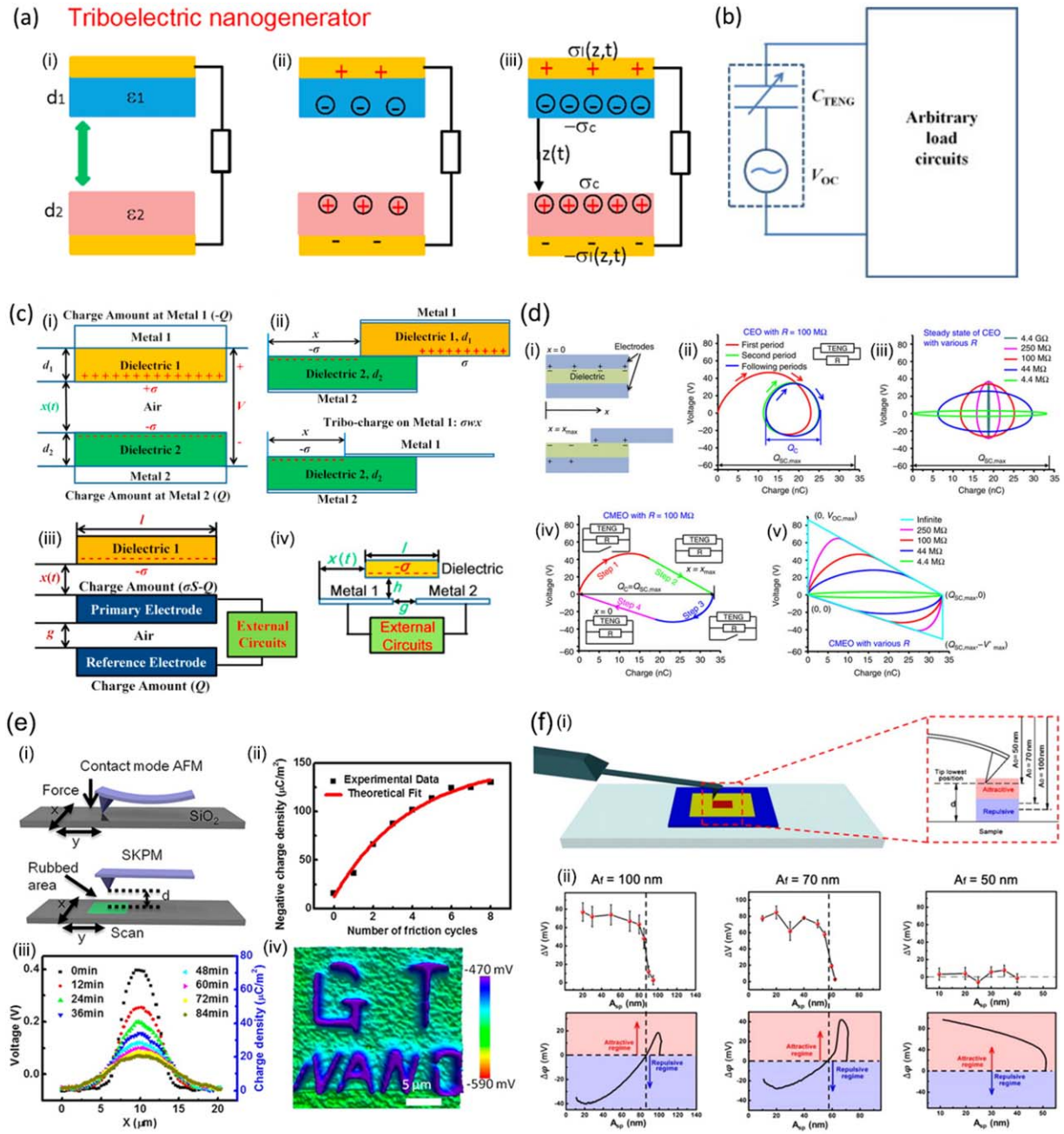

Figure 4. Triboelectric nanogenerators. (a) Working mechanism of TENGs with the increase of contact cycles. Adapted from Ref. 48, https://doi.org/10.1016/j.mattod.2016.12.001, https://creativecommons.org/licenses/by-nc-nd/4.0/. (b) Equivalent electrical circuit of a TENG. Reprinted from Ref. 49, Copyright (2014), with permission from Elsevier. (c) Theoretical models of different modes of TENG. Adapted with permission from Refs. 50–53. Ref. 50:Copyright (2014) John Wiley & Sons. Ref. 52:Copyright (2015), with permission from Elsevier. Ref. 53:Copyright (2015) John Wiley & Sons. (d) *V*–*Q* plots for different operation cycles of a lateral-sliding-mode TENG. Adapted from Ref. 54. (e) *In situ* quantitative study of nanoscale triboelectrification and patterning. Reprinted with permission from Ref. 55, Copyright (2013) American Chemical Society. (f) Surface potential measurement using Kevin Probe Force Microscopy. Reprinted with permission from Ref. 56, Copyright (2016) American Chemical Society. [Color figure can be viewed at wileyonlinelibrary.com]

transferred between materials in mutual contact after their separation.[47] The fundamental working principle of TENGs is then based on the combination of contact electrification (CE), which provides static polarized charges, and electrostatic induction which allows the conversion of mechanical energy to electricity through the use of proper electrodes [Figure 4(a); (i–iii)].[48] Contact electrification is one of the most frequently experienced effects in daily life since almost all substances exhibit a triboelectrification effect (metals, polymers, silk, cotton, wood, etc.) and in the last 15 years several materials and device design have been implemented in order to improve the charge density and the output performances. Polymers are materials of election for TENGs since (i) several compounds are present in both the positive tail [electron-losing,

(+)] and the negative tail [electron-accepting, (–)] of the triboelectric series (categorizing materials according to their capability to gain or lose electric charges upon contact with other surfaces) and (ii) are intrinsically and highly mechanically flexible.

The equivalent circuit of a TENG is reported in Figure 4(b), where the capacitance, C_{TENG}, originates from the capacitance between the two electrodes, and the open-circuit voltage term, V_{OC}, originates from the separation of polarized tribo-charges.[49] C_{TENG} and V_{OC} are functions of (i) moving distance (x) and (ii) structural parameters, being independent from velocity and acceleration.[51] Therefore, the energy conversion mechanism of TENGs can harvest mechanical motion in a wide range of frequencies and consistencies. Depending on the electrostatic induction process, TENGs can be classified according to their operation mode [Figure 4(c); (i–iv)][50–53,57] and a system of standard has been introduced by Zi *et al.* to allow comparison among different devices. Examples of *V-Q-x* plots, where V is the built-up voltage, Q is the total transferred charges Q, and x is the relative displacement between the triboelectric layers, are reported in Figure 4(d).[54] In general, TENGs based on paired-electrode perform better than TENGs based on single electrodes of the same size and materials, and the contact-separation mode is better than sliding.[58]

In order to quantify the triboelectrification process of TENGs at the nanoscale, Zhou *et al.* demonstrated an *in situ* method by using atomic force microscopy.[55] The atomic force microscopy operates in contact mode under a normal contact force of 120 nN on a SiO_2 film [Figure 4(e)], inducing a friction pattern that was then characterized *in situ* by scanning Kelvin potential microscopy.[55] The surface charge density was derived as a function of the number of friction cycles [Figure 4(e); (ii)] after the surface potential profiles [as shown in Figure 4(e); (iii)] were generated from scanning Kelvin potential microscopy images.[55] Recently, Li *et al.* decoupled CE from the surface potential measurement in order to improve the accuracy of insulator and semiconductor characterization during topography scans by using Kelvin probe force microscopy (KPFM).[56] A dual-pass KPFM measurement was performed using two passes in one scan line—the first pass being a topography scan in tapping mode, and the second pass being the tip-sample potential difference method.[56] During the first pass, CE between the probe tip and sample causes significant changes in the surface potential, thus reducing the accuracy of the measurement.[56] The schematics in Figure 4(f)—(i) show the dual-pass scanning ranges where the marked red area indicates the first pass topography scan range and the inset displays a cross-sectional diagram of the tip-sample interaction forces.[56] They found that by decreasing the free vibration amplitude (A_0), increasing the scanning amplitude (A_{sp}), and replacing the KPFM probe with a cantilever with a smaller spring constant, the surface potential change induced by CE could be decoupled from the measurement.[56]

The surface charge density on the triboelectric surfaces can be improved through chemical modification. In the following we report some examples of functionalization used in the last five years. Ion-injection was used by Wang *et al.* to deposit negative ions on the surface of a fluorinated ethylene propylene (FEP) layer, working as the negative triboelectric surface in the device.[59] While the charge density of an electrode-free, unmodified FEP film would be limited by the dielectric breakdown of air, the deposition of negative ions induce the electrostatic transfer of the same number of electrons from the attached electrode to the ground.[59] This process, depicted in Figure 5(a), results in the bottom electrode being positively charged with the same charge density as the FEP layer.[59] By using a stable injection of CO_3^-, NO_3^-, NO_2^-, O_3^-, and O_2^- ions, the power density was improved 25-fold to a maximum of 315 W/m^2, and the maximum surface charge density improved almost five times from −50 to −240 μC/m^2.[59] Self-assembled monolayers of alkanethiols with various functional groups attached [Figure 5(b)] were used to functionalize gold electrodes. Self-assembled monolayer modifies the surface chemical potential of the gold, thus deeply affecting the contact in triboelectrification performance. An improvement of the surface charge density from 68 to 140 μC/m^2 and of the open-circuit voltage from 270 to 560 V was measured.[60]

Another approach used to strengthen the electrical output performance of triboelectric PNG consists in modifying the design parameters. Zhu *et al.* designed a rotating TENG [Figure 5(c)] capable of harvesting ambient mechanical motion and a power-supplying system that provides a continuous DC source at constant voltage.[61] In such construction, the output power was found to linearly increase with the TENG area, and the short circuit current linearly decreases as the central angle increases.[61] The efficiency of this rotating TENG was found to be ~24%, and the output current did not decay even after 10 million cycles of AC.[61] A shape-adaptive micro-grating TENG was developed by Zhu *et al.* using polymer thin films with complementary linear electrode [Figure 5(d)].[62] The original design enables harvesting of the mechanical energy produced while sliding straight or curved surfaces and possesses both flexibility and mechanical robustness. The addition of polytetrafluoroethylene (PTFE) NPs on the triboelectric surfaces, reduces wear phenomena, and nearly 50% of conversion efficiency was achieved.[62] Additional improvement of the efficiency can be obtained by limiting the mechanisms of energy dissipation during solid-solid friction such as by using liquid–metal interfaces as reported by Tang *et al.* [Figure 5(e)]. In such case, an instantaneous energy conversion efficiency of 70.6% was achieved by using a large variety of polymers such as polyimide (Kapton), PTFE, poly(ethylene terephthalate), and parylene as triboelectric surface.[63] Conversion efficiency up to 85% was instead demonstrated by Xie *et al.* using a grating-structured, freestanding triboelectric layer of FEP.[64] An acrylic sheet was used as substrate and nanorods were created on the FEP surface through inductive coupling plasma reactive ion etching to enhance contact triboelectification.[64] The working principle relies on the coupling of CE and in-plane-sliding-induced charge transfer, in which a potential drop occurs when the FEP grating is displaced from the equilibrium position.[64] Human sliding is enough to generate electricity capable of lighting up 60 commercial LEDs instantaneously and the mechanical energy of a person's leg performing a walking motion, as depicted in Figure 5(f)—(ii), may be harvested.[64]

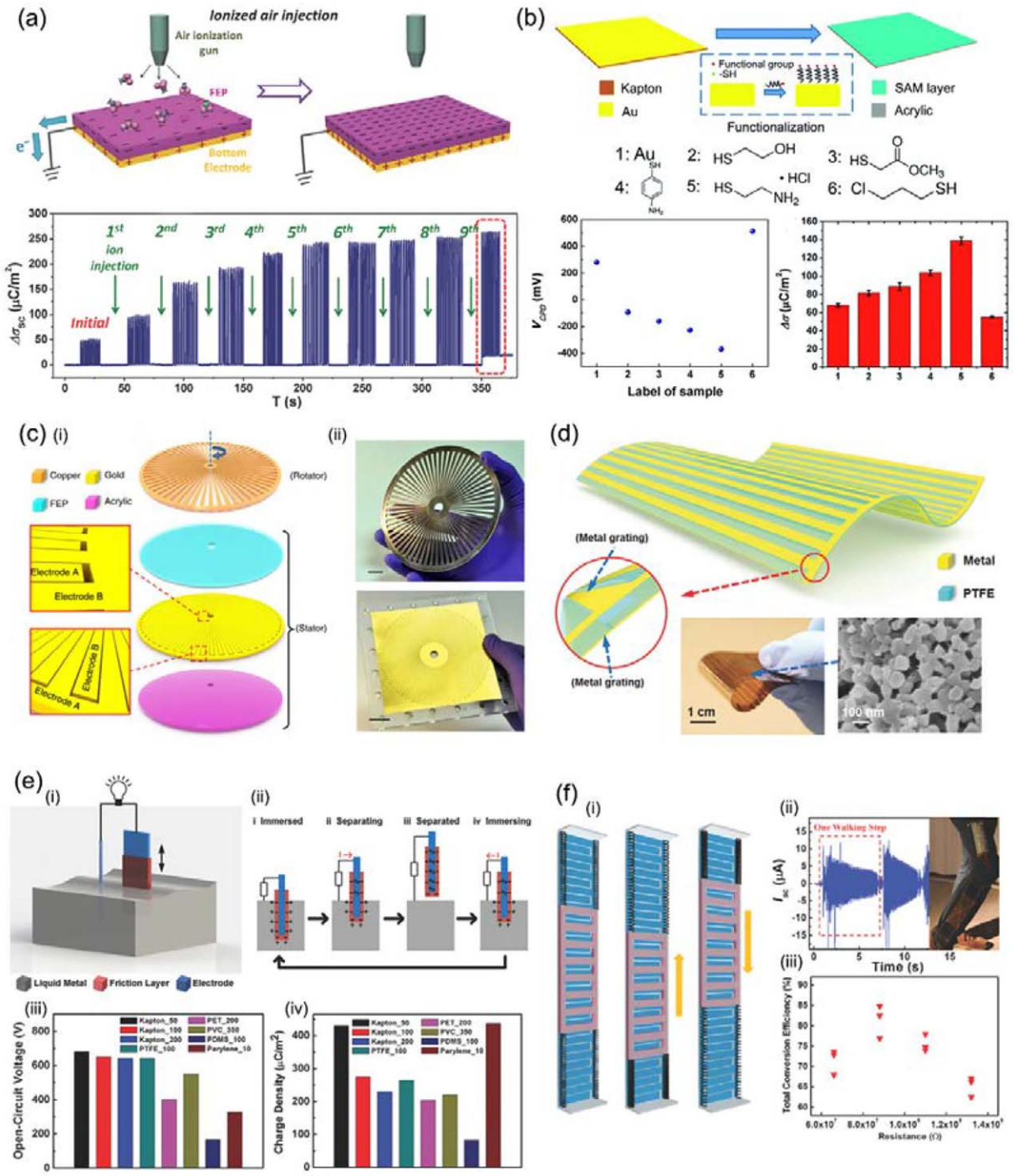

Figure 5. Toward high-performance TENGs. (a) Maximizing surface charge density for TENGs by ionized-air injection. Adapted with permission from Ref. 59, Copyright (2014) John Wiley & Sons. (b) Molecular surface functionalization to enhance the power output of TENGs. Adapted with permission from Ref. 60, Copyright (2016) The Royal Society of Chemistry. (c) Radial-arrayed rotary electrification for high performance triboelectric generator. Reprinted by permission from Macmillan Publishers Ltd (Ref. 61), Copyright (2014) (d) A thin-film-based high-power TENG through micrograting sliding electrification. Adapted with permission from Ref. 62, Copyright (2014) John Wiley & Sons. (e) A liquid-metal-based TENG with an instantaneous energy conversion efficiency of 70.6%. Adapted with permission from Ref. 63, Copyright (2014) John Wiley & Sons. (f) A grating-structured freestanding TENG with a total conversion efficiency of 85%. Adapted with permission from Ref. 64, Copyright (2014) John Wiley & Sons. [Color figure can be viewed at wileyonlinelibrary.com]

Electrostatic Generators

Electrostatic generators (ESGs) operate through either the triboelectric effect or electrostatic induction, and were among the first mechanical energy harvesting electric generators ever conceptualized. They produce static electricity, or electricity at high voltage and low continuous current. The "friction machine" as

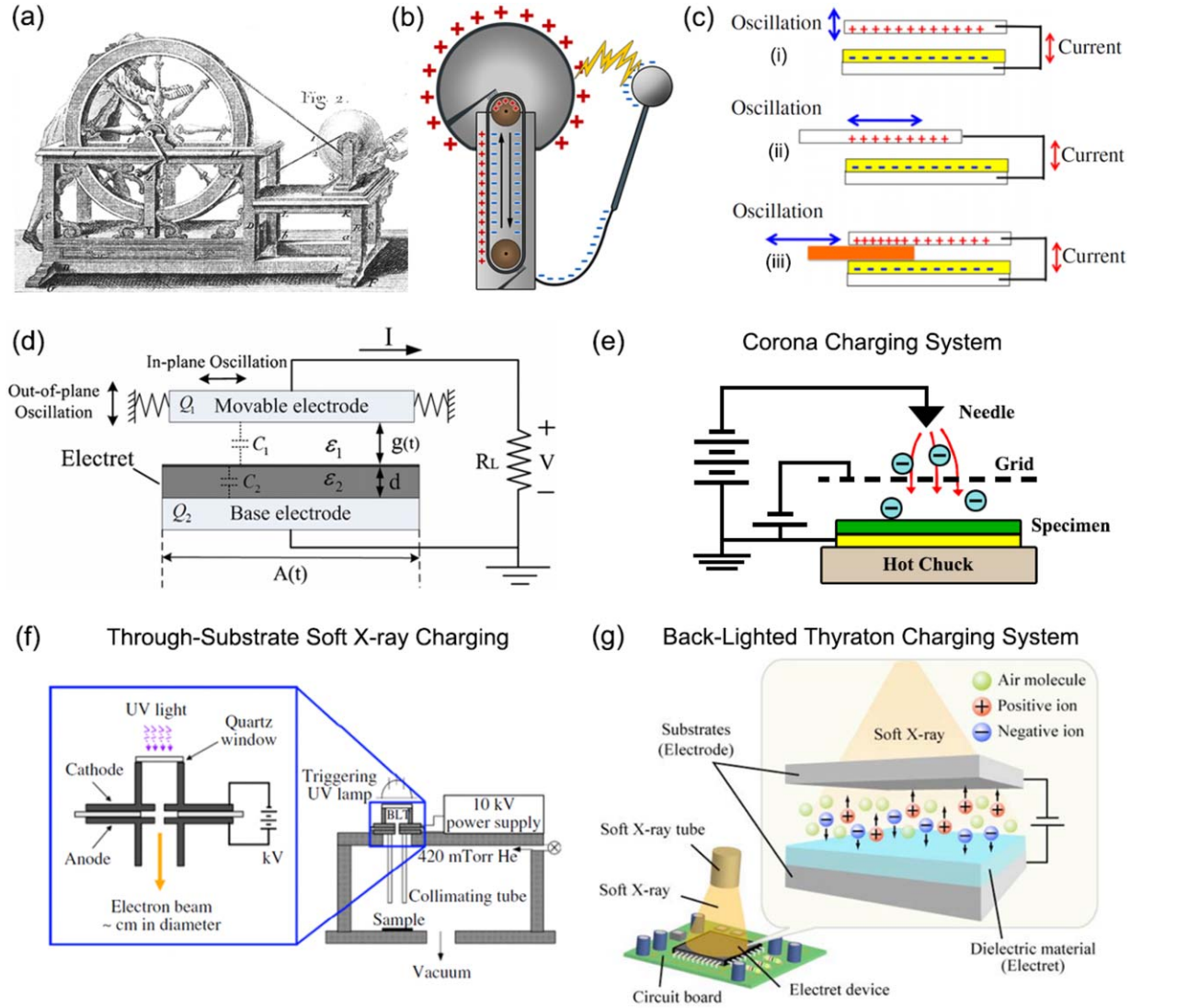

Figure 6. Electrostatic/electret generator. (a) Sketch of early friction machine. Courtesy of the MIT Libraries, Institute Archives, and Special Collections. Vail Collection. Essai sur l'électricité des corps, Abbé Jean Antoine Nollet, 1765. (b) Schematic of Van de Graff machine. (c) Operation principle of electret generators. Reprinted with permission from 65, Copyright (2011) John Wiley & Sons. (d) Equivalent electrical circuit of an electret generator with both in-plane and out-of-plane operation modes. Reprinted from Ref. 66, http://iopscience.iop.org/0960-1317/24/6/065022, Copyright IOP Publishing. Reproduced with permission. All rights reserved (e) Corona electret charging system. (f) Through-substrate soft X-ray electret charging system. Reprinted from Ref. 67. Courtesy of Prof. Y.-C. Tai. (g) Back-lighted thyratron electret charging system. Reprinted from Ref. 68. Courtesy of Dr. K. Hagiwara. [Color figure can be viewed at wileyonlinelibrary.com]

depicted in Figure 6(a), was one of the first prototypes of ESG, and operate by triboelectric effect. A glass sphere accumulates charges when rubbed against skin or cloth thus producing static electricity. Generators were further advanced in the 19th century and one of the most important machine capable of producing high-voltage was the Van de Graaff generator depicted in Figure 6(b). This was invented in 1929,[69] and was based on the contact between an insulating belt pulled between two rollers of different materials, one of which surrounded by a hollow metal sphere. Van de Graaff generators work by combining triboelectric chargers formed by contact of dissimilar materials with electrostatic induction used to magnify the produced charges. To expand the range of operational frequency, in 1978 electret generators were first proposed[65] to harvest low frequency vibrations that EMGs could not convert into energy due to their higher mechanical resonant frequencies.[70] The construction of electret generators is relatively simple, with a stationary electrode beneath the electret and a movable electrode separated by an air gap. While capacitors exhibit induced polarization temporarily, electrets hold a quasi-permanent electrostatic field that can be stable for tens of years. Electret materials include polymers, waxes, and quartz. Figure 6(c) shows three different operation modes of electret generators, gap-closing [top of Figure 6(c)], in plane oscillation [middle of Figure 6(c)], and an in-plane oscillation of a high permittivity material placed in the air gap [bottom of Figure 6(c)].[65] As the top movable electrode oscillates in-plane or out-of-plane, the displacement between the two plates causes a capacitance variation, generating an

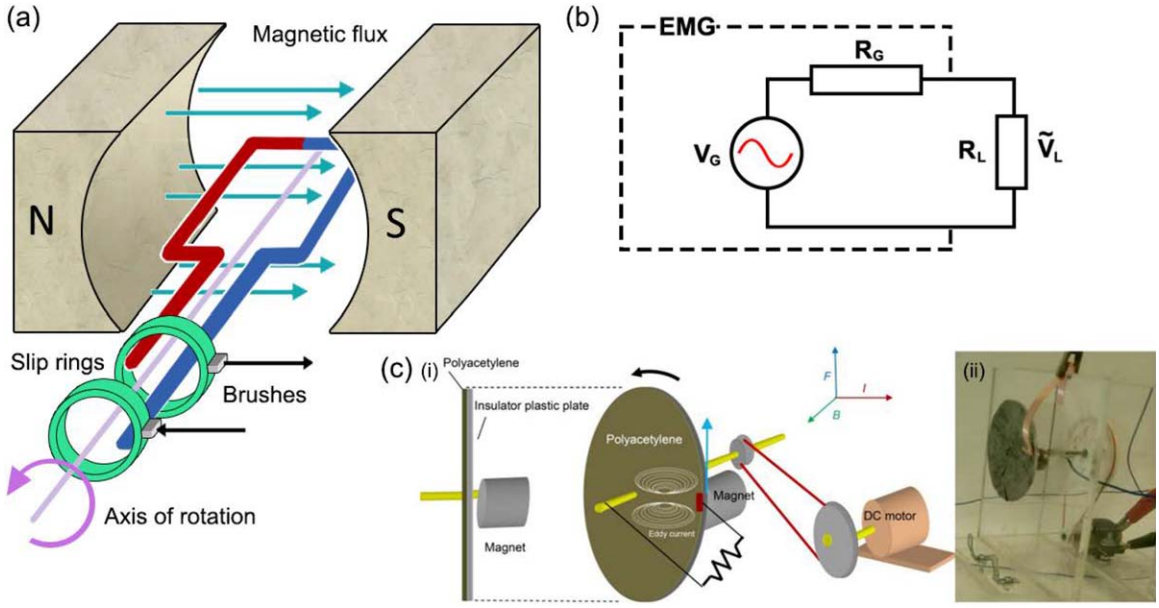

Figure 7. Electromagnetic generator. (a) Schematic of an alternating-current generator. (b) Equivalent electrical circuit of an EMIG in which EMG represents the EMIG, R_G is the internal generator resistance, R_L is the load resistance, V_G is the generator open-circuit voltage, and V_L is the generator on-load voltage. (c) Soliton electric generators based on conducting polymers. Adapted from Ref. 77, DOI: 0.1088/1757–899X/54/1/012019. [Color figure can be viewed at wileyonlinelibrary.com]

alternating current (ac), as shown in Figure 6(d).[66] Similarly to ESGs, electret generators produce electricity through capacitance changes in the presence of a charge bias from either precharging an electret or an external voltage source.[66] The methods used to charge electret generators are depicted in Figure 6(e–g), which includes a corona charging system,[71] back-lighted thyratron charging system,[67] and through-substrate soft X-ray charging system.[68] In corona charging, a charged needle electrode induces ionization of the air around it through a potential gradient, and the ions drift toward a low-field grid that keeps the electric field uniform during charging.[72] In back-lighted thyratron charging, a UV light pulse applied to the back of a precharged hollow-back cathode plate initiates a pulsed electron beam towards the electret.[73] Finally, in soft X-ray charging, air molecules are ionized through electromagnetic radiation up to tens of keV, and the ions are separated by charge through an electric field and deposit onto oppositely charged electrets.[68] Electret generators may require precharging in order to operate, but they remain a powerful tool to harvest environmental vibrations with long-term charge stability. The sensitivity and efficiency of electrets in-plane sensors, actuators, and generators depends largely on gap spacing.[74] A microelectromechanical systems (MEMS) electret generator was developed using a high-performance perfluoropolymer material, with the air gap controlled through a repulsive electrostatic force.[74] The seismic mass and bottom substrate are both patterned with a precharged electret of amorphous fluorinated polymer CYTOP, which produces a repulsive force of 0.1 mN mm^{-2}, enough to levitate the seismic mass suspended by parylene springs.[74] Using an electromagnetic shaker at 63 Hz with an acceleration of 2 *g*, a total power output of 1.0 μW was achieved.[74] With precise air gap control using a long-lasting electrostatic repulsive force, the mechanical wear lifetime and effective vibration harvesting of electret generators have been greatly improved. CYTOP is an optimal polymer for electret formation due to its high surface charge density of 1.3 mC m^{-2} (in 15-μm thick films), and may be enhanced even further with the addition of aminosilanes, forming additional charge traps.[75]

Electromagnetic Generators

The majority of modern devices that convert mechanical energy to electricity operate by using electromagnetic induction generators (EMIGs), in which electric current is generated in a conductor moved through a magnetic field.[76] In Figure 7(a), a simple ac EMIG is depicted, consisting of a wire coil rotating around one axis between the opposing poles of two magnets. When the coil rotates, the associated flux of magnetic field changes, resulting in an electromotive force between the ends of the coil. Slip rings transfer the alternating electromotive force to an external circuit through the attached carbon brushes, which convert ac output into dc output, making it a DC-EMIG.[78] An example of equivalent electrical circuit of an EMIG is reported in Figure 7(b).

MEMS EMIGs are generally based on single crystal silicon and used to harvest ambient vibrations.[79] A polymer-based, low-cost alternative MEMS was proposed by Yang *et al.* and consists of a polymer beam with multiple magnets attached, vibrating atop a printed circuit board substrate with multiple coils.[80] High frequencies of vibration are required for the polymer beam generator to harvest mechanical energy, ranging from 369 to 1184 Hz and producing a total output power of 1.157 μW from three coils connected serially.[80] Recently a polymer EMIG was fabricated by using a conductive polymer film on a polyacrylonitrile circular board in place of a metal wheel.[77] The polymer EMIG, depicted in Figure 7(c), produced a low voltage (0.2 mV) as

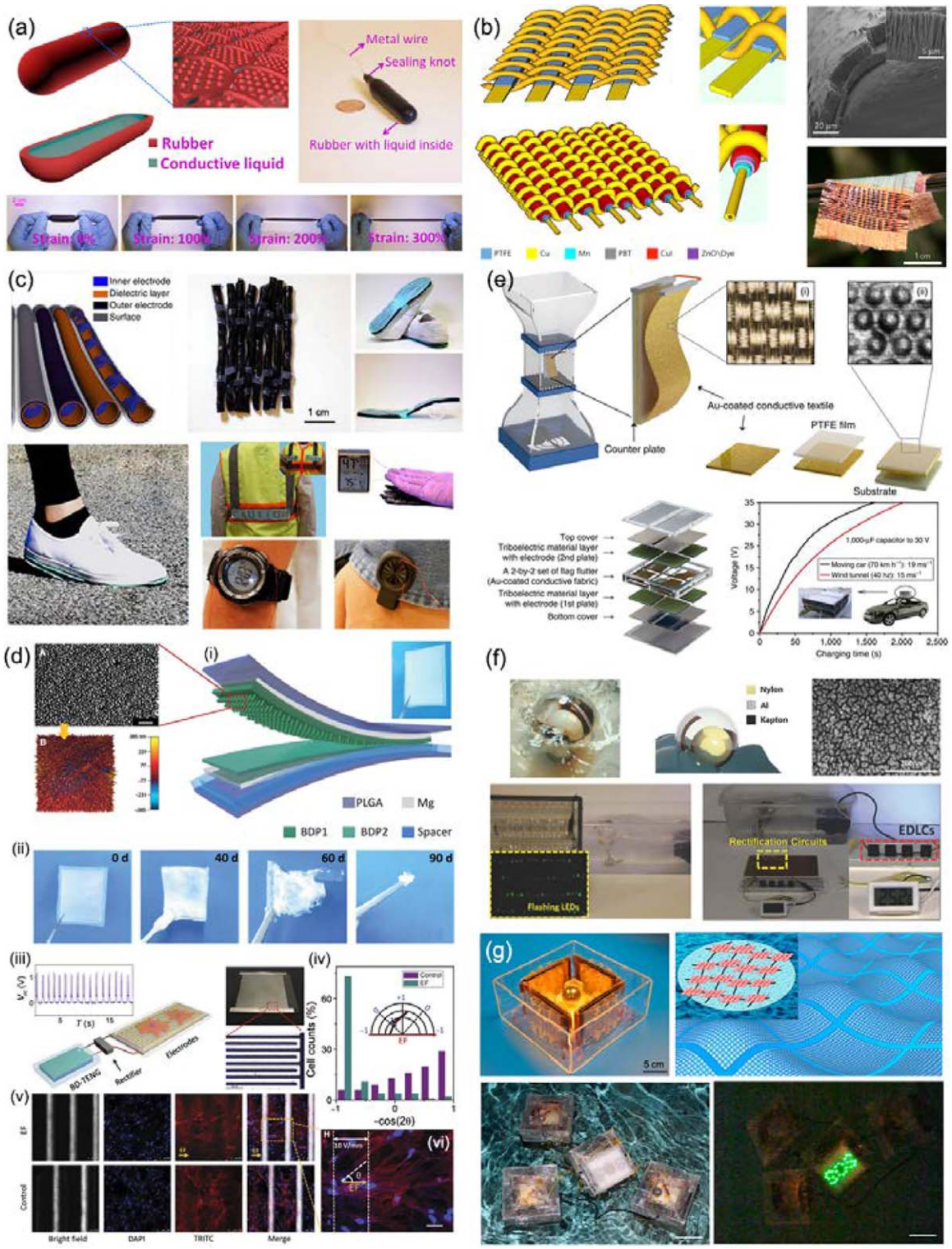

Figure 8. TENG as sustainable power sources. (a) Conductive-liquid-based, shape-adaptive, stretchable TENG for biomechanical energy harvesting. Adapted from Ref. 85. (b) Microcable structured textile for simultaneously harvesting solar and mechanical energy. Reprinted by permission from Macmillan Publishers Ltd (Ref. 86), Copyright (2016). (c) Wearable, tube-like TENG for harvesting biomechanical energy from daily motions. Adapted from Ref. 87. (d) Biodegradable TENG as a life-time designed implantable power source. Adapted from Ref. 88. (e) Flutter-driven TENG for harvesting wind energy. Reprinted by permission from Macmillan Publishers Ltd: [Nature Communications] (Ref. 89), Copyright (2014). (f) Fully enclosed rolling spherical TENG for harvesting low-frequency water wave energy. Reprinted with permission from Ref. 90, Copyright (2015) John Wiley & Sons. (g) TENG networks for harvesting large-scale blue energy. Reprinted with permission from Ref. 91, Copyright (2015) American Chemical Society. [Color figure can be viewed at wileyonlinelibrary.com]

well as low current.[77] Generally, the output power of EMIGs decays upon decreasing the operational frequency, and conventional ac generator can hardly operate at frequencies below 50–60 Hz.[81] However, in nature, most of the vibration frequencies are below 10 Hz (see for example, ocean waves and human motions) thus making these sources of mechanical energy largely unusable with this type of generators.[81] In a study performed by Zhang *et al.* a rotating DC-EMIG using a similar model as the one reported in Figure 7(a) was found to have a peak power output of 102.6 μW, which was lower than the peak output of a rotating DC-TENG (140.4 μW).[82] The lighter material used in the DC-TENG also resulted in a higher maximum power per unit mass and per unit volume compared to the DC-EMIG.[82] When compared to an EMIG, TENGs possess more flexibility in device design due to less restrictive mechanisms of operation, wider material selection, and self-powering capabilities. In the near future, TENGs have the potential to be used just as frequently as EMIGs and in a wider variety of applications.

APPLICATIONS: OPPORTUNITIES AND CHALLENGES

NGs may be used for a wide variety of applications due to their broadly adaptable levels of integration, flexibility in the mechanical triggering mechanism, and sensing capabilities. The use of elastic and deformable materials strongly contributes to expanding the device design options and the scalability perspectives. Here, we report some example of applications with focus on those approaches that show large-scale capability. Due to their intrinsic mechanical flexibility, lightness, and compactness piezoelectric PNG have a marked potential application in wearable and stretchable electronics,[6] for the detection of biomechanical motions and personal healthcare,[23] for sensing,[83] and they can be used as direct source of energy or combined with properly designed storage elements.[7,84] A shape-adapting TENG made using a conductive liquid electrode and an elastic polymer cover [Figure 8(a)], may be used as a self-powered biomechanical motion sensor.[85] As the liquid electrode conforms to the shape of its container and the rubber has a large deformation range, the PNG was capable of withstanding a strain of 300% without degradation of electrical properties.[85] Energy-harvesting textiles have also been developed to create more comfortable and pliable materials for wearable PNG.[85,86] Using low-cost and lightweight polymer fibers mixed with wool fibers, a hybrid solar cell and TENG fabric was produced in order to harvest solar and mechanical energy simultaneously.[86] Figure 8(b) shows schematics of the fabric TENG, constructed from PTFE strips and copper electrodes, and the photovoltaic textile, constructed from wire-shaped photoanodes and counter electrodes.[86] A SEM image of a photoanode and a photograph of the hybrid textile mixed with colored wool fibers are shown on the right end of Figure 8(b). Under sunlight exposure and mechanical excitation, an adult palm-sized piece of the hybrid power textile is able to charge a 2 mF capacitor to 2 V in 1 min, continuously powering a digital watch, and charging a cell phone.[86] Stability tests showed that the electric output of the TENG fabric diminished to 73.5% of its original value as humidity increased from 10% to 90%, but this degradation can be reversed if the textile is dried.[86] Encapsulation could represent an effective solution to reduce humidity effects. A highly adaptable tube-shaped [Figure 8(c)] TENG was developed by Wang *et al.* for powering wearable technology such as fitness trackers and watches through harvesting the biomechanical energy produced from human motion.[87] The NG can be woven or incorporated into a variety of clothing items and shoes due to its thinness (2–7 mm) and flexibility and can power LED warning signs, digital watches, fitness trackers, and temperature and humidity meters.[87]

A biodegradable TENG based on poly(L-lactide-*co*-glycolide), poly(3-hydroxybutyric acid-*co*-3-hydroxyvaleric acid), poly(caprolactone), and poly(vinyl alcohol) and bioresorbable metals [Figure 8(d)] may be used (i) as short-term implantable biomedical device, as it works for over 24 h *in vivo* at 3 V and is almost biodegraded completely within 72 h[88] or (ii) to drive the orientation of the cytoskeletons of neuron cells in the direction of the electric field [Figure 8(d); (iii)].[88]

An omnipresent source of mechanical energy on earth comes from wind. So far, it has been harnessed using windmills and wind turbines. A lightweight flutter-driven PNG was fabricated by using a conducting Au-coated flag and a dielectric PTFE plate to harvest wind energy through a contact-separation mechanism.[89] A wind tunnel containing the flutter-driven TENG is depicted in Figure 8(e), showing surface characteristics of both the Au-coated textile flag and the counter plate. It was found that at higher wind speeds, the higher fluttering speed increases contact force between the flag and the plate, increasing V_{OC}, I_{SC}, and the charging rate.[89] When mounted on a car moving 70 km h^{-1}, the device is capable to charge a 1000 μF capacitor to 30 V in about 17 min.[89] The device design is simple in construction, lightweight, and low cost.

TENGs can also offer a safe, cheap, scalable, and low-frequency energy harvesting solution to harnessing "blue energy," or the kinetic energy of ocean waves. A rolling-structured, freestanding TENG was constructed using a Nylon ball and Kapton film in an enclosed spherical shell, capable of harnessing even low frequency wave motion [Figure 8(f)].[90] Once paired with a series of four electric double-layer capacitors and bridge rectifiers, the PNG was capable of charging the electric double-layer capacitors to 2.4 V after a few hours of oscillation in water. With a different device design, TENGs based on PTFE nanowires in contact with a nanopore-enhanced aluminum electrode [Figure 8(g)] and connected in a network would be capable of producing 1.15 MW if spread in an area of 1 km^2 at the ocean surface. These networks would eliminate the need for anchoring structures and the heavy machinery necessary to operate EMG blue energy harvesters.[91] Polymer-based TENGS are also largely used as sensors. Among others we recall here, pressure sensors,[92] strain sensors capable of detecting human body movements and displacement on a person moving in a vehicle,[93] weight sensor and smart seat belt sensors,[93] and chemical sensors.[94]

Results so far achieved and in particular, the realization of triboelectric generator exceeding 85% of the energy conversion efficiency, indicate that PNGs have concrete potentiality for use in everyday life. However, several issues are yet to be solved

before the devices can be ready for commercialization. First, the mechanism behind triboelectrification is still debated and not yet clearly rationalized. Although several efforts have been made to investigate the maximum surface charge density and the process of charge dissipation and diffusion, results are still preliminary and the controversy over the process of charge generation and its effects on energy harvesting remains unsettled. Another straightforward issue is how to systematically improve the output performance of TENGs and make them reproducible and relevant for large-scale applications. In this respect, the optimization of the material choice and of the device design is still worth studying. In addition, for practical applications, the NG is one of the key element constituting the harvesting system which also include: power management circuits, signal processing circuits, and energy storage elements. The optimization of the power generation unit is the first step toward the construction of efficient harvesting systems and both the power management and energy storage components are expected to deeply impact on the overall efficiency.[95]

CONCLUSIONS

This review summarizes recent progress in piezoelectric, triboelectric, and electrostatic/electromagnetic technologies that rely on mechanics based on polymeric materials. The material chemistries, operational principles, and device design strategies have been detailed and related to the device performances. The unique opportunities and challenges for use in real-life applications have been highlighted.

The ever growing demand for interconnection, both among people and among objects, is expected to (i) increase the collective need of energy [13 terawatts (TW) calculated in 2005 and 30 TW expected in 2050][96] and to (ii) deeply modify the perception of energy in real-life applications through the introduction of self-powered and wearable systems. In a world where inanimate objects and moveable elements interact with the external environment, for example, through systems of sensors, and will uniquely be identifiable and capable of data transmission, the main keywords will be safety, sustainability, efficiency, and portability. Mechanical energy harvesting based on polymers can potentially fulfill all of these requirements, also allowing the exploitation of sources of energy otherwise largely wasted such as ambient vibrational and mechanical energy, human motion, water flows, etc. For instance, while most of wind turbines and hydroelectric generators currently in use are based on standard electric generators that require a regular and high frequency input, the development, at large scale, of mechanical NG would allow one to additionally harvest energy at low frequency and with high flexibility in terms of the triggering mechanism and consistency. However, notwithstanding technologies for the massive deposition of polymers, including tools and equipments for the realization of nanomaterials at large scale, are already available on the market, the commercialization perspectives of NGs cannot be clearly traced yet. Key challenges in the field are (i) the capability to create new lines of production with the required flexibility for the final device assembly (realization of different device geometries and material choice, multiple device assembly, low temperature processing for contact deposition, etc.) thus capable to reflect one of the main advantages of this technology which can span over a broad variety of triggering mechanism, sources of energy and device design, (ii) the achievement of good mechanical stability and durability for long operation time, and (iii) the development of efficient integrated systems. So far, hundreds of articles have been published on PNGs [Clarivate Analytics Web of Science. Copyright clarivate analytics 2016. All rights reserved. Topic keywords "polymer," "nanogenerator" (accessed May 22, 2017)] and approximately the same number of patents have been issued in the last 15 years [WIPO PATENTSCOPE, full text keyword: polymer and nanogenerator, https://patentscope.wipo.int/ (accessed May 22, 2017)] thus clearly indicating that the basic research in the field is advancing in parallel to the investigation of specific solutions to the technological issues related to PNG products and processing lines. The advancement in materials, fabrication techniques, and device design will certainly lead to further improvement in available technological alternatives and afford new opportunities for application across wide ranging areas.

ACKNOWLEDGMENTS

D.P. and L.P. acknowledge the European ResearchCouncil for supporting, under the European Union's SeventhFramework Programme (FP7/2007-2013), the ERC Starting Grant "NANO-JETS" (grant agreement n. 306357).

REFERENCES

1. Wang, Z. L.; Song, J. H. *Science* **2006**, *312*, 242.
2. Qi, Y.; Kim, J.; Nguyen, T. D.; Lisko, B.; Purohit, P. K.; McAlpine, M. C. *Nano Lett.* **2011**, *3*, 1331.
3. Persano, L.; Camposeo, A.; Tekmen, C.; Pisignano, D. *Macromol. Mater. Eng.* **2013**, *298*, 504.
4. Jung, S.; Lee, J.; Hyeon, T.; Lee, M.; Kim, D.-H. *Adv. Mater.* **2014**, *26*, 6329.
5. Kholkin, A. L.; Pertsev, N. A.; Goltsev, A. V. In Piezoelectric and Acoustic Materials for Transducer Applications; Safari, A., Akdoğa, E. K., Eds.; Springer: New York, **2008**; Chapter 2, p 17.
6. Wu, H.; Huang, Y.; Xu, F.; Duan, Y.; Yin, Z. *Adv. Mater.* **2016**, *28*, 9881.
7. Xue, X.; Wang, S.; Guo, W.; Zhang, Y.; Wang, Z. L. *Nano Lett.* **2012**, *12*, 5048.
8. Sharma, T.; Je, S.-S.; Gill, B.; Zhang, J. X. J. *Sens. Actuators* **2012**, *177*, 87.
9. Persano, L.; Catellani, A.; Dagdeviren, C.; Ma, Y.; Guo, X.; Huang, Y.; Calzolari, A.; Pisignano, D. *Adv. Mater.* **2016**, *28*, 7633.
10. Fang, F.; Wang, X.; Lin, T. *J. Mater. Chem.* **2011**, *21*, 11088.
11. Persano, L.; Dagdeviren, C.; Maruccio, C.; De Lorenzis, L.; Pisignano, D. *Adv. Mater.* **2014**, *26*, 7574.
12. Duan, Y. Q.; Huang, Y. A.; Yin, Z. P.; Bu, N. B.; Dong, W. T. *Nanoscale* **2014**, *6*, 3289.

13. Persano, L.; Dagdeviren, Su, Y.; Zhang, Y.; Girardo, S.; Pisignano, D.; Huang, Y.; Rogers, J. A. D. *Nat. Commun.* **2013**, *4*, 1633.
14. Baniasadi, M.; Huang, J.; Xu, Z.; Moreno, S.; Yang, X.; Chang, J.; Quevedo-Lopez, M. A.; Naraghi, M.; Minary-Jolandan, M. *ACS Appl. Mater. Interfaces* **2015**, *7*, 5358.
15. Kanik, M.; Aktas, O.; Sener Sen, H.; Durgun, E.; Bayindir, M. *ACS Nano* **2014**, *8*, 9311.
16. Chen, X.; Tian, H.; Li, X.; Shao, J.; Ding, Y.; An, N.; Zhou, Y. *Nanoscale* **2015**, *7*, 11536.
17. Mao, Y.; Zhao, P.; McConohy, G.; Yang, H.; Tong, Y.; Wang, X. *Adv. Energy Mater.* **2014**, *4*, 1301624.
18. Liu, X.; Ma, J.; Wu, X.; Lin, L.; Wang, X. *ACS Nano* **2017**, *11*, 1901.
19. Gutierrez, M. C. G.; Linares, A.; Hernandez, J. J.; Rueda, D. R.; Ezquerra, T. A.; Poza, P.; Davies, R. *J. Nano Lett.* **2010**, *10*, 1472.
20. Bhavanasi, V.; Kusuma, D. Y.; Lee, P. S. *Adv. Energy Mater.* **2014**, *4*, 1400723.
21. Shin, S. H.; Kim, Y. H.; Lee, M. H.; Jung, J. Y.; Nah, J. *ACS Nano* **2014**, *8*, 2766.
22. Park, J.; Kim, M.; Lee, Y.; Lee, H. S.; Ko, H. *Sci. Adv.* **2015**, *1*, 1500661.
23. Tong, W.; Zhang, Y.; Zhang, Q.; Luan, X.; Lv, F.; Liu, L.; an, Q. *Adv. Funct. Mater.* **2015**, *25*, 7029.
24. Park, K.-I.; Xu, S.; Liu, Y.; Hwang, G.-T.; Kang, S.-J. L.; Wang, Z. L.; Lee, K. *J. Nano Lett.* **2010**, *10*, 4939.
25. Siddiqui, S.; Kim, D.-I.; Duy, L. T.; Nguyen, M. T.; Muhammad, S.; Yoon, W.-S.; Lee, N.-E. *Nano Energy* **2015**, *15*, 177.
26. Valsecchi, R.; Viganò, M.; Levi, M.; Turri, S. *J. Appl. Polym. Sci.* **2006**, *102*, 4484.
27. Brutchey, R. L.; Morse, D. E. *Angew. Chem. Int. Ed.* **2006**, *45*, 6564.
28. Lin, M.-F.; Lee, P. S. *J. Mater. Chem. A* **2013**, *1*, 14455.
29. Persano, L.; Camposeo, A.; Di Benedetto, F.; Stabile, R.; Laera, A. M.; Piscopiello, E.; Tapfer, L.; Pisignano, D. *Adv. Mater.* **2012**, *24*, 5320.
30. Di Benedetto, F.; Camposeo, A.; Persano, L.; Laera, A. M.; Piscopiello, E.; Cingolani, R.; Tapfer, L.; Pisignano, D. *Nanoscale* **2011**, *3*, 4234.
31. El Achaby, M.; Arrakhiz, F. Z.; Vaudreuil, S.; Essassi, E. M.; Qaiss, A.; Bousmina, M. J. *Appl. Polym. Sci.* **2013**, *127*, 4697.
32. Huang, L.; Lu, C.; Wang, F.; Wang, L. *RSC Adv.* **2014**, *4*, 45220.
33. Kim, K.; Zhu, W.; Qu, X.; Aaronson, C.; McCall, W. R.; Chen, S.; Sirbuly, D. J. *ACS Nano* **2014**, *8*, 9799.
34. McCall, W. R.; Kim, K.; Heath, C.; La Pierre, G.; Sirbuly, D. J. *ACS Appl. Mater. Interfaces* **2014**, *6*, 19504.
35. Wu, N.; Cheng, X.; Zhong, Q.; Zhong, J.; Li, W.; Wang, B.; Hu, B.; Zhou, J. *Adv. Funct. Mater.* **2015**, *25*, 4788.
36. Datta, A.; Choi, Y. S.; Chalmers, E.; Ou, C.; Kar-Narayan, S. *Adv. Funct. Mater.* **2017**, *27*, 1604262.
37. Lee, B.-S.; Park, B.; Yang, H.-S.; Han, J. W.; Choong, C.; Bae, J.; Lee, K.; Yu, W.-R.; Jeong, U.; Chung, U.-I. *ACS Appl. Mater. Interfaces* **2014**, *6*, 3520.
38. Jeong, C. K.; Lee, J.; Han, S.; Ryu, J.; Hwang, G.-T.; Park, D. Y.; Park, J. H.; Lee, S. S.; ByunKo, M. S. H.; Lee, K. J. *Adv. Mater.* **2015**, *27*, 2866.
39. Li, B.; Zhang, F.; Guan, S.; Zheng, J.; Xu, C. *J. Mater. Chem. C* **2016**, *4*, 6988.
40. Lu, X.; Qu, H.; Skorobogatiy, M. *ACS Nano* **2017**, *11*, 2103.
41. Chen, X.; Shao, J.; An, N.; Li, X.; Tian, H.; Xu, C.; Ding, Y. *J. Mater. Chem. C* **2015**, *3*, 11806.
42. Fuh, Y.-K.; Chen, P.-C.; Huang, Z.-M.; Ho, H.-C. *Nano Energy* **2015**, *11*, 671.
43. Park, T.; Kim, B.; Kim, Y.; Kim, E. *J. Mater. Chem. A* **2014**, *2*, 5462.
44. Fuh, Y.-K.; Kuo, C. C.; Huang, Z. M.; Li, S. C.; Liu, E. R. *Small* **2016**, *12*, 1875.
45. Lee, J.-H.; Lee, K. Y.; Gupta, M. K.; Kim, T. Y.; Lee, D.-Y.; Oh, J.; Ryu, C.; Yoo, W. J.; Kang, C.-Y.; Yoon, S.-J.; Yoo, J.-B.; Kim, S.-W. *Adv. Mater.* **2014**, *26*, 765.
46. Alluri, N. R.; Saravanakumar, B.; Kim, S.-J. *ACS Appl. Mater. Interfaces* **2015**, *7*, 9831.
47. Fan, F. R.; Tian, Z. Q.; Wang, Z. L. *Nano Energy* **2012**, *1*, 328.
48. Wang, Z. L. *Mater. Today* **2017**, *20*, 74.
49. Niu, S.; Zhou, Y. S.; Wang, S.; Liu, Y.; Lin, L.; Bando, Y.; Wang, Z. L. *Nano Energy* **2014**, *8*, 150.
50. Niu, S.; Liu, Y.; Wang, S.; Lin, L.; Zhou, Y. S.; Hu, Y.; Wang, Z. L. *Adv. Funct. Mater.* **2014**, *24*, 3332.
51. Niu, S.; Wang, S.; Lin, L.; Liu, Y.; Zhou, Y. S.; Hu, Y.; Wang, Z. L. *Energy Environ. Sci.* **2013**, *6*, 3576.
52. Niu, S.; Liu, Y.; Chen, X.; Wang, S.; Zhou, Y. S.; Lin, L.; Xie, Y.; Wang, Z. L. *Nano Energy* **2015**, *12*, 760.
53. Niu, S.; Liu, Y.; Wang, S.; Lin, L.; Zhou, Y. S.; Hu, Y.; Wang, Z. L. *Adv. Mater.* **2013**, *25*, 6184.
54. Zi, Y.; Niu, S.; Wang, J.; Wen, Z.; Tang, W.; Wang, Z. L. *Nat. Commun.* **2015**, *6*, 8376.
55. Zhou, Y. S.; Liu, Y.; Zhu, G.; Lin, Z. H.; Pan, C.; Jing, Q.; Wang, Z. L. *Nano Lett.* **2013**, *13*, 2771.
56. Li, S.; Zhou, Y.; Zi, Y.; Zhang, G.; Wang, Z. L. *ACS Nano* **2016**, *10*, 2528.
57. Wang, Z. L.; Chen, J.; Lin, L. *Energy Environ. Sci.* **2015**, *8*, 2250.
58. Wang, Z. L.; Lin, L.; Chen, J.; Niu, S.; Zi, Y. Triboelectr. Nanogenerators **2016**, 185.
59. Wang, S.; Xie, Y.; Niu, S.; Lin, L.; Liu, C.; Zhou, Y. S.; Wang, Z. L. *Adv. Mater.* **2014**, *26*, 6720.
60. Wang, S.; Zi, Y.; Zhou, Y. S.; Li, S.; Fan, F.; Lin, L.; Wang, Z. L. *J. Mater. Chem. A* **2016**, *4*, 3728.
61. Zhu, G.; Chen, J.; Zhang, T.; Jing, Q.; Wang, Z. L. *Nat. Commun.* **2014**, *5*, 3426.
62. Zhu, G.; Zhou, Y. S.; Bai, P.; Meng, X. S.; Jing, Q.; Chen, J.; Wang, Z. L. *Adv. Mater.* **2014**, *26*, 3718.

63. Tang, W.; Jiang, T.; Fan, F. R.; Yu, A. F.; Zhang, C.; Cao, X.; Wang, Z. L. *Adv. Funct. Mater.* **2015**, *25*, 3718.
64. Xie, Y.; Wang, S.; Niu, S.; Lin, L.; Jing, Q.; Yang, J.; Wu, Z.; Wang, Z. L. *Adv. Mater.* **2014**, *26*, 6599.
65. Suzuki, Y. *IEEJ Trans.* **2011**, *6*, 101.
66. Tao, K.; Liu, S.; Lye, S. W.; Miao, J.; Hu, X. *J. Micromech. Microeng.* **2014**, *24*, 065022.
67. Suzuki, Y. *IEEJ Trans* **2011**, *6*, 101.
68. Hagiwara, K.; Honzumi, M.; Goto, M.; Tajima, T.; Yasuno, Y.; Kodama, H.; Kidokoro, K.; Kashiwagi, K.; Suzuki, Y. PowerMEMS; Washington, DC, **2009**.
69. Furfari, F. A. *IEEE Ind. Appl. Mag.* **2005**, *11*, 10.
70. Lo, H. W.; Whang, R.; Tai, Y. C. Proceedings IEEE 20th Int. Conf. on Micro Electro Mechanical Systems (MEMS'07), Hyogo, Japan; **2007**; p 859.
71. Sakane, Y.; Suzuki, Y.; Kasagi, N. *J. Micromech. Microeng.* **2008**, *18*, 104011.
72. Giacometti, J. A.; Oliveira, O. N. *IEEE Trans. Electr. Insul.* **1992**, *27*, 924.
73. Tai, Y. C.; Hsu, T. Y.; Hsieh, W. H. U.S. Pat. 0,033,670 (**2001**).
74. Suzuki, Y.; Miki, D.; Edamoto, M.; Honzumi, M. *J. Micromech. Microeng.* **2010**, *20*, 104002.
75. Kashiwagi, K.; Okano, K.; Miyajima, T.; Sera, Y.; Tanabe, N.; Morizawa, Y.; Suzuki, Y. *J. Micromech. Microeng.* **2011**, *21*, 125016.
76. Beeby, S. P.; Tudor, M. J.; White, N. M. *Meas. Sci. Technol.* **2006**, *17*, R175.
77. Goto, H. IOP Conf. Ser.: Mater. Sci. Eng. **2014**, *54*, 012019.
78. Hoong, F. C. U.S. Pat. 6,121,705 (**2000**).
79. Koukharenko, E.; Tudor, M. J.; Beeby, S. P. *Mater. Lett.* **2008**, *62*, 651.
80. Yang, B.; Lee, C.; Xiang, W.; Xie, J.; He, J. H.; Kotlanka, R. K.; Low, S. P.; Feng, H. *J. Micromech. Microeng.* **2009**, *19*, 035001.
81. Zi, Y.; Guo, H.; Wen, Z.; Yeh, M. H.; Hu, C.; Wang, Z. L. *ACS Nano* **2016**, *10*, 4797.
82. Zhang, C.; Tang, W.; Han, C.; Fan, F.; Wang, Z. L. *Adv. Mater.* **2014**, *11*, 3580.
83. Zhang, L.; Yu, X.; You, S.; Liu, H.; Zhang, C.; Cai, B.; Xiao, L.; Liu, W.; Guo, S.; Zhao, X. *Appl. Phys. Lett.* **2015**, *107*, 242901.
84. Lee, J.-H.; Kim, J.; Kim, T. Y.; Hossain, M. S. A.; Kim, S. W.; Kim, J. H. *J. Mater. Chem. A* **2016**, *4*, 7983.
85. Yi, F.; Wang, X.; Niu, S.; Li, S.; Yin, Y.; Dai, K.; Zhang, G.; Lin, L.; Wen, Z.; Guo, H.; Wang, J.; Yeh, M. H.; Zi, Y.; Liao, Q.; You, Z.; Zhang, Y.; Wang, Z. L. *Sci. Adv.* **2016**, *2*, e1501624.
86. Chen, J.; Huang, Y.; Zhang, N.; Zou, H.; Liu, R.; Tao, C.; Fan, X.; Wang, Z. L. *Nat. Energy* **2016**, *1*, 16138.
87. Wang, J.; Li, S.; Yi, F.; Zi, Y.; Lin, J.; Wang, X.; Xu, Y.; Wang, Z. L. *Nat. Commun.* **2016**, *7*, 12744.
88. Zheng, Q.; Zou, Y.; Zhang, Y.; Liu, Z.; Shi, B.; Wang, X.; Jin, Y.; Ouyang, H.; Li, Z.; Wang, Z. L. *Sci. Adv.* **2016**, *2*, e1501478.
89. Bae, J.; Lee, J.; Kim, S. M.; Ha, J.; Lee, B. S.; Park, Y. J.; Choong, C.; Kim, J. B.; Wang, Z. L.; Kim, H. Y.; Park, J. J.; Chung, U. I. *Nat. Commun.* **2014**, *5*, 4929.
90. Wang, X.; Niu, S.; Yin, Y.; Yi, F.; You, Z.; Wang, Z. L. *Adv. Energy Mater.* **2015**, *5*, 1501467.
91. Chen, J.; Yang, J.; Li, Z.; Fan, X.; Zi, Y.; Jing, Q.; Guo, H.; Wen, Z.; Pradel, K. C.; Niu, S.; Wang, Z. L. *ACS Nano* **2015**, *9*, 3324.
92. Fan, F. R.; Lin, L.; Zhu, G.; Wu, W.; Zhang, R.; Wang, Z. L. *Nano Lett.* **2012**, *12*, 3109.
93. Zhang, S. L.; Lai, Y. C.; He, X.; Liu, R.; Zi, Y.; Wang, Z. L. *Adv. Funct. Mater.* **2017**, *27*, 1606695.
94. Lin, Z. H.; Zhu, G.; Zhou, Y. S.; Yang, Y.; Bai, P.; Chen, J.; Wang, Z. L. *Angew. Chem. Int. Ed.* **2013**, *52*, 1.
95. Niu, S.; Wang, X.; Yi, F.; Zhou, Y. S.; Wang, Z. L. *Nat. Commun.* **2015**, *6*, 8975.
96. Service, R. F. *Science* **2005**, *309*, 548.